Influence of Sheathing-Fastener Connection Stiffness on the Design Strength of Cold-Formed Steel Wall Panels

Sivaganesh Selvaraj, Ph.D.[1]; and Mahendrakumar Madhavan, Ph.D., P.E., M.ASCE[2]

Abstract: This paper investigates the bracing effect of sheathing fastener connection on point-symmetric shaped cold formed steel (CFS) studs through full-scale laboratory tests. The test parameters include slenderness of the CFS stud, fastener connection spacing, and sheathing thickness. The test results indicate that the bracing effect of the particle cement board has significantly enhanced the moment capacity of the CFS stud, nevertheless, this was not completely captured by the current design specifications of American Iron and Steel Institute (AISI). The detailed discussion on the unsuitability of the current AISI design method in determining the design moment capacity and failure modes of the sheathed CFS wall stud is presented. In addition, the PCB-fastener connection demand check shows that the provided sheathing configurations are adequate to brace the CFS studs from biaxial bending, which is in contrast compared to the experimental results. Therefore, a new test setup is proposed to accurately determine the stiffness of the sheathing fastener connections to formulate a reliable design method.
DOI: 10.1061/(ASCE)ST.1943-541X.0002709.

Author keywords: Sheathing-fastener connections; Cold-formed steel wall panels; Fastener-connection stiffness; Full-scale tests; Design expressions.

Introduction

The structural behavior of the cold-formed steel (CFS) member is difficult to predict owing to its complex shapes and interacting buckling failure modes. Nonetheless, the cold-formed steel construction practices have reached a stage that it can replace any structural member in the conventional construction. The primary impediment to success is neither the construction technology nor the design guidelines, but rather the fundamental understanding of the behavior of various structural systems such as the bracing effect of the sheathing and built-up members. The current study is focused on the bracing effect of sheathing boards on cold-formed steel structural members. These sheathing boards are inherently present in the structural system as an external covering. The bracing effects of sheathing in CFS wall systems are mostly unknown, especially for the various shapes of the CFS member and loading cases. A fundamental understanding of the failure modes is necessary for the development of reliable design specification for CFS structural members.

Background on the Sheathed CFS Wall Panel Design

Early studies to investigate the potential of the sheathing boards for bracing effect were conducted at Cornell University by Winter (1960) and Winter et al. (1972). The investigation by Winter suggested new guidelines for the sheathing braced design called $2a$ rule. The definition of the $2a$ rule is that the unbraced length of the CFS stud subjected to axial compression reduces from KL to twice of the fastener spacing ($2a$) owing to the bracing effect of sheathing. In this case L is the unbraced length of the CFS member, K is the effective length coefficient, and a is spacing between two fastener connections (center–to–center). In the present work, the spacing between the fasteners is denoted as d_f. This $2a$ rule was adopted in the American Iron and Steel Institute (AISI) design specifications (AISI 1983, 1986; Yu 2000; AISI 2012) with the following limitations: (1) sheathing fastener connection shall have adequate rigidity to arrest the instability of the CFS stud; (2) the sheathing configuration (material, fastener spacing, and thickness) shall be identical on both the sides of the CFS wall panel [Fig. 1(a)] or if the sheathing configuration nonidentical [Fig. 1(b)] then the weaker sheathing material should be considered in the design; and (3) the fastener connection spacing shall not exceed 305 mm (12 in.).

Recently, the AISI (2013) has developed a fastener connection stiffness-based design method to predict the structural contribution of the sheathing board and relaxed the limitations of the $2a$ rule. The objective of stiffness-based sheathing braced design method is to simplify the design complexities in the CFS design by introducing a software analysis method and include the structural effect of sheathing irrespective of the sheathing configuration (identical and nonidentical) and fastener spacings. The fastener connection stiffness components of the AISI design method are shown in Fig. 1(c). According to AISI, there are three idealized stiffnesses present at the particle cement board (PCB)-fastener connection location, namely, lateral translational stiffness (k_x), out-of-plane stiffness (k_y), and rotational stiffness (k_ϕ). The definition and the experimental methodology used to determine the fastener connection stiffnesses are summarized in Table 1. Though this design method was validated only for the case of compression loading, it was recommended for both compression and out-of-plane loading cases (AISI 2013). The recent comprehensive investigations revealed that the stiffness-based design method by AISI (2013) for considering

[1]Postdoctoral Fellow, Dept. of Civil Engineering, Indian Institute of Technology Hyderabad, Kandi, Sangareddy, Telangana 502 285, India. ORCID: https://orcid.org/0000-0003-0782-7003. Email: ce13p1009@iith.ac.in

[2]Associate Professor, Dept. of Civil Engineering, Indian Institute of Technology Hyderabad, Kandi, Sangareddy, Telangana 502 285, India (corresponding author). ORCID: https://orcid.org/0000-0002-3144-5278. Email: mkm@iith.ac.in

Note. This manuscript was submitted on October 8, 2019; approved on February 19, 2020; published online on July 21, 2020. Discussion period open until December 21, 2020; separate discussions must be submitted for individual papers. This paper is part of the ***Journal of Structural Engineering***, © ASCE, ISSN 0733-9445.

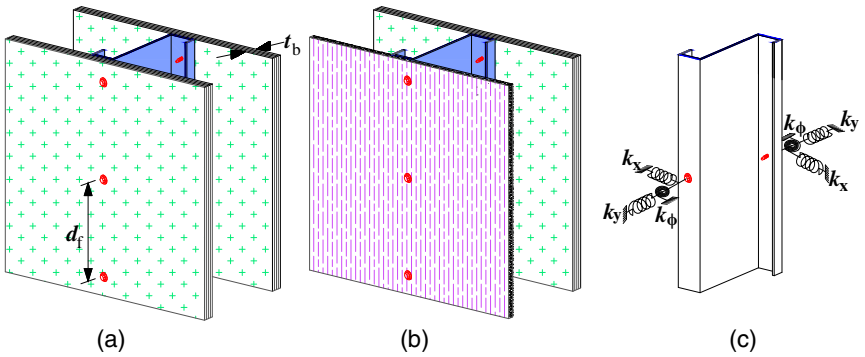

Fig. 1. Fastener connection bracing: (a) identical sheathing-fastener connection configuration; (b) nonidentical sheathing-fastener connection configuration; and (c) stiffness at the sheathing-fastener connection.

Table 1. Fastener connection stiffness components as per AISI

Stiffness component as per AISI (2013)	Definition	Formalized from
k_x—Lateral-translational stiffness	The resistance offered by the sheathing-fastener connection against the weaker axis buckling of the CFS stud.	The test setup was developed by Winter (1960), applies the pulling force to the identically sheathed CFS studs, and the total shear developed at each sheathing–fastener connection is equivalent to the force applied. The expression for determination of this stiffness was formulated by Vieira and Schafer (2012b).
k_y—Out-of-plane stiffness	The additional flexural stiffness of the sheathing board added to the major-axis bending rigidity of the CFS wall stud.	This stiffness can be determined by assuming three different composite actions between the sheathing and CFS structural member. However, the simple and appropriate method is to assume the full-composite action and add the flexural stiffness of the sheathing with the CFS stud (Vieira 2011; Selvaraj and Madhavan 2019b).
k_ϕ—Rotational stiffness	The resistance against the cross-sectional twist of the CFS stud.	The test setup was developed Winter et al. (1972), applies the pulling force to rotate the CFS studs with respect to the sheathing faster connection location. The expression for determination of this stiffness was formulated by Schafer et al. (2011).

the structural contribution of sheathing in CFS wall panel design is unreliable because of the incorrect failure mode predictions (Selvaraj and Madhavan 2018b, c). It was concluded that the incorrect prediction of failure modes of the sheathed CFS wall panels were because of the following: (1) the stiffness components are categorized only based on the test setup simulating the failure modes of the CFS wall stud subjected to axial compression; and (2) although it appears that the methodologies used to determine the fastener connection stiffnesses are appropriate (Table 1), the application of all three idealized stiffnesses overestimates the bracing effect of sheathing. The investigation by Selvaraj and Madhavan (2018b) suggests modifying the fastener connection stiffness combinations based on the failure mode of the CFS stud as shown in Fig. 2 rather than incorporating all three stiffnesses simultaneously in the software analysis. Nevertheless, the appropriateness of the modified design method by Selvaraj and Madhavan (2018b) was not verified for the point-symmetric CFS wall studs sheathed with particle cement board. Therefore, the purpose of the present study is to explore the structural behavior of the PCB sheathed point-symmetric CFS studs. Although similar investigations were carried out recently (Selvaraj and Madhavan 2019b, j, e, l, d), it is necessary to carry out more detailed investigations on sheathed CFS wall panels to develop a robust and accurate design procedure. The major advantage of developing a sheathing braced design method is that it will result in an economical construction by eliminating the need for additional steel bracing.

Design Parameters

The experimental study on full-scale sheathed CFS wall panels was carried out to explore the structural behavior of PCB-fastener connections. The CFS wall panels are fabricated with a single stud. The parameters considered are (1) five different CFS studs with varying slenderness (λ_l, λ_e, and λ_d), (2) two different thicknesses of particle cement board (t_b), and (3) fastener spacing (d_f), totaling 20 full-scale test panels. Five different CFS studs include four different thicknesses with different material properties; however, the material properties are incorporated in the slendernesses (λ_l, λ_d, and λ_e) as nondimensional design parameters. The terms λ_l, λ_d, and λ_e denote the local, distortional, and global slendernesses of the point-symmetric CFS stud, respectively. It should be noted that only one specimen is tested for exploring the influence of each design parameter (either sheathing thickness or fastener spacing or slenderness of the CFS stud). However, a reliability study is carried out for the obtained results. The cross-sectional dimensions of the point-symmetric CFS studs are explicitly designed to investigate the bracing effect of PCB sheathing for various slenderness of CFS sections. This is precisely because the previous studies on sheathed wall panels indicate that the structural contribution of sheathing is substantial for the CFS wall studs that are vulnerable to global failure and insignificant for locally slender ones (Miller and Peköz 1994; Telue and Mahendran 2001; Ye et al. 2016; and Zhang et al. 2016). Therefore, the Z02 point-symmetric CFS stud was designed to fail in both biaxial bending ($\lambda_e \gg 1$) and local

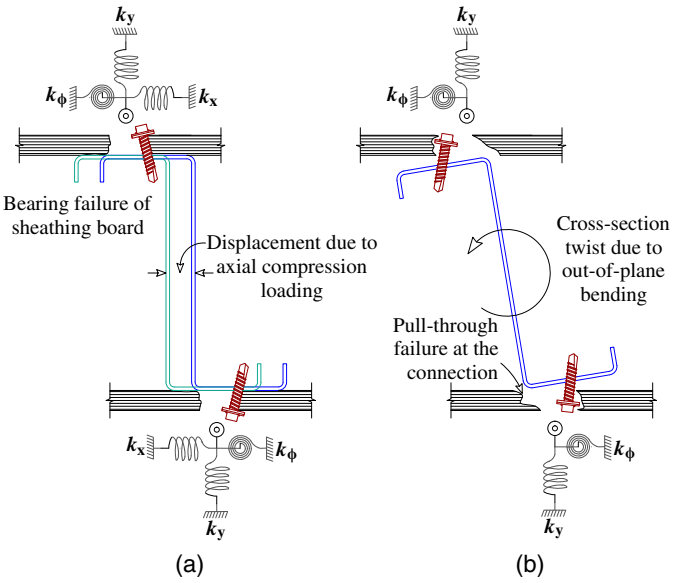

Fig. 2. Fastener connection stiffness based bracing design concepts: (a) AISI method for axial compression; and (b) design method for out-of-plane loading according to Selvaraj and Madhavan (2018b).

Table 2. Material properties of cold-formed steel studs from the tensile tests

CFS coupon	E_s (GPa)	f_y (MPa)	f_u (MPa)	ε_f (%)
CFS–1.0 mm	221.3	330.1	425	18
	210.9	365.2	426.4	17.6
	216.6	357.7	436.9	16.8
CFS–1.5 mm	212.2	377.4	440	16.1
	217.9	376.4	439.2	18.3
	202.7	378.3	442.8	18.2
CFS–2.0 mm	201.5	377.6	417.6	17.3
	214.8	386.4	420.1	17.6
	206.5	370.4	417.5	18.2
CFS–2.5 mm	215.8	329.9	419.8	18
	213.8	336.8	426.9	17.6
	211.9	335.6	421.6	17

Note: E_s = Young's modulus of steel; f_y = yield strength of steel; f_u= ultimate tensile strength; and ε_f = strain at fracture.

buckling ($\lambda_l \gg 1$) while other CFS studs are designed to fail in biaxial bending only ($\lambda_e \gg 1$). It should be noted that no CFS stud was designed to fail in distortional buckling ($\lambda_d \ll 1$), simply because the previous literature indicated that the distortional buckling of the CFS studs is not influenced by the sheathing bracing effect (Vieira and Schafer 2012a). This cross-section optimization was carried out by keeping the length of the wall stud as constant. The unbraced length of the CFS stud was chosen conservatively as the current AISI standard S210 (AISI 2012) on floor and roof system design recommends providing additional steel bracing only when the length of the wall stud is more than 2,440 mm (8 ft). In the current study, the unbraced length test specimen is 2,250 mm and as a consequence the fastener connection stiffness required to hinder the global buckling of the longer member is lower than the shorter member (Yura 2001). Hence, the results obtained from experiments will be conservative when it is adopted to 2,440 mm (8 ft) long CFS stud.

Material properties and actual cross-sectional dimensions of the point-symmetric CFS wall studs are summarized in Tables 2 and 3, respectively. In each set of the sheathed CFS wall panel, four different sheathing configurations are varied. The sheathed CFS wall studs are labeled (e.g., ZL01-12-300) as follows: CFS Stud number-sheathing thickness (t_b)-fastener spacing (d_f).

Material Property Test

The necessary material properties of the PCB sheathing board and CFS stud for the determination of the design strength and fastener connection stiffnesses are obtained from tensile tests. A total of 12 CFS coupon tests were carried out with three samples in each thickness as shown in Table 2. Similarly, three samples for each thickness were tested for PCB sheathing board. The particle cement board is a sheet that contains 62% cement and 28% wood particle with a density of 12.5 kN/m^3 [mixture proportion as per IS 14276 (IS 1995) and ASTM (2012)]. The CFS stud coupon dimensions were arrived from ASTM E8 (ASTM 2013) and PCB sheathing was tested as a strip of size 6 in. long and 1 in. wide (150 × 25 mm). The PCB sheathing was attached with a metal sheet on both the sides (front and back) and at both ends of the coupon specimen for force application (grip). The bond length between the PCB and metal tab is based on the minimum bond length suggested by ASTM D2718 (ASTM 2018c). The tensile loading on the CFS and PCB coupons were applied through a constant axial displacement at a rate of 0.5 mm/min according to the ASTM standards (ASTM 2013, 2015). The Young's modulus (E_s) and tensile modulus (E_g) of the CFS coupons and PCB coupons, respectively were calculated from the strain gauge readings. The material properties obtained from tensile tests are summarized in Tables 2 and 4, respectively.

Fastener Connection between Sheathing and CFS Stud

In general, the stiffness of the fastener connection is significantly influenced by the type of fastener used for connecting the sheathing

Table 3. Cross-sectional dimensions of cold-formed steel studs (C–channels)

Specimen	Depth h (mm) (out-to-out)	Breadth b (mm) (out-to-out)	Thickness t (mm)	Lip l_p (mm)	Section slenderness		
					λ_l	λ_d	λ_e KL = 2,250 mm
ZL01	95	50	1.5	15	0.65	0.76	1.45
Z02	90	50	1.0	—	2.28	—	1.79
ZL03	83	33	2.0	18	0.36	0.46	1.69
Z04	118	25	2.5	—	0.44	—	2.32
Z05	122	28	1.5	—	0.9	—	2.72

Note: h = depth of CFS stud (web); b = breadth of the CFS stud (flange); t = thickness of the CFS stud; l_p = depth of the lip in CFS stud; $\lambda_l = (F_y/F_{crl})^{0.5}$; $\lambda_d = (F_y/F_{crd})^{0.5}$; and $\lambda_e = (F_y/F_{cre})^{0.5}$.

Table 4. Material properties of PCB board (sheathing material) obtained from the tensile tests

PCB coupon thickness	Tensile modulus, E_g (MPa)	Ultimate tensile, strength F (MPa)
8 mm	2,583.6	1.78
	2,909.7	1.76
	2,630.0	1.60
12 mm	2,604.0	1.76
	2,846.4	1.78
	2,485.8	1.72
Mean	2,676.6	1.73
Standard deviation	164.72	0.07
Coefficient of variation	0.0615	0.040

board and the CFS stud. However, the material properties of the fastener do not affect as the PCB is expected to fail because of its lesser modulus and powdery material composition (cement and wood particles). Therefore, fastener type was selected based on the previous research and according to the design guidelines. The fastener used in the present study is of hexagonal head and No. 6 type as per ASME (2003) as shown in Fig. 3(a). In addition, to avoid premature failure and to smoothly distribute the force developed at the connection, a steel cum rubber washer was used as per the suggestions of the Steel Framing Guide (SFA et al. 2007) and Selvaraj and Madhavan (2019f, i, a). Further, the fastener was driven on the PCB board and CFS stud such that it is not overdriven on the surface of the PCB board [Fig. 3(c)] and a minimum of pitch threads are inserted beyond the CFS stud [Fig. 3(b)] [NAHB 1997; ASTM C954 (ASTM 2018a); and ASTM C1002 (ASTM 2018b)].

Experimental Program

Test Setup

It is necessary that the test setup should be devised such that the test results are not influenced by any other factors since the objective of the proposed work is to explore the structural contribution of the PCB-fastener connection when the CFS wall panel is subjected to out-of-plane loading. The present study did not use the typical end track connections at the ends of the test specimens, because the connection at the ends may fail in pull-out of screws because of the pulling force (bending downward and creating tension force at the connections) that is applied to the panel. When such failure happens at the connections, the true bracing effect of the sheathing boards cannot be captured. Therefore, a unique support fixture has been developed instead of having a traditional track or hold-down connections at the support ends as shown in Fig. 4(a). The uniqueness of the support fixture is that it can hold the sheathed point-symmetric CFS studs in position, arrest the CFS studs from twisting, and avoids slippage at the support ends. In addition, the fixture avoids any concentric loading on the sheathed CFS panels at the supports and the support fixture simulates the behavior of the wall panel that has parallel CFS studs.

The testing program was carried out using a 250 kN actuator test frame as shown in Figs. 4(a) and 5. Displacement control mode (constant rate of 0.3 mm/min) was used for the application of out-of-plane loading. The displacement application was paused at several stages of loading for about 3 min to ensure that the loading is static. The test specimen was loaded at two loading points with an intermediate distance of 800 mm, which is almost equal to the one-third length of the sheathed CFS wall stud [2,250 mm—Fig. 4(a)]. The out-of-plane deflection was applied to the CFS wall panels such that the center of gravity of the load passes through the plane of web of the point-symmetric (Z-shaped) CFS stud. But the principal axis of the point-symmetric shaped CFS stud is inclined to the plane of the web [Fig. 4(d)]. However, it is the usual way of loading point-symmetric CFS studs (Pi et al. 1999). The simply supported loading condition was achieved by providing rotation free half-rounds as shown in Figs. 4(e) and 5(b).

Validation of the Test Setup

Although the loading arrangements and support fixtures appear to be logical (Figs. 4 and 5), it is necessary to verify if indeed whether the test setup simulates the desired support conditions. The

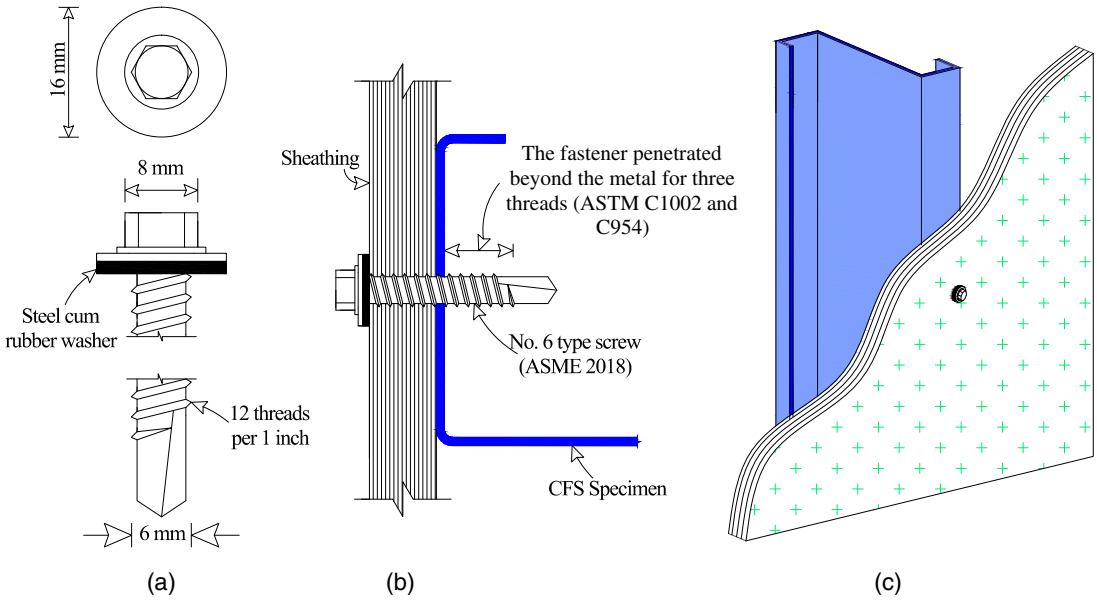

Fig. 3. Details of the sheathing-fastener connection: (a) fastener type; (b) connecting method; and (c) view of the fastener connection.

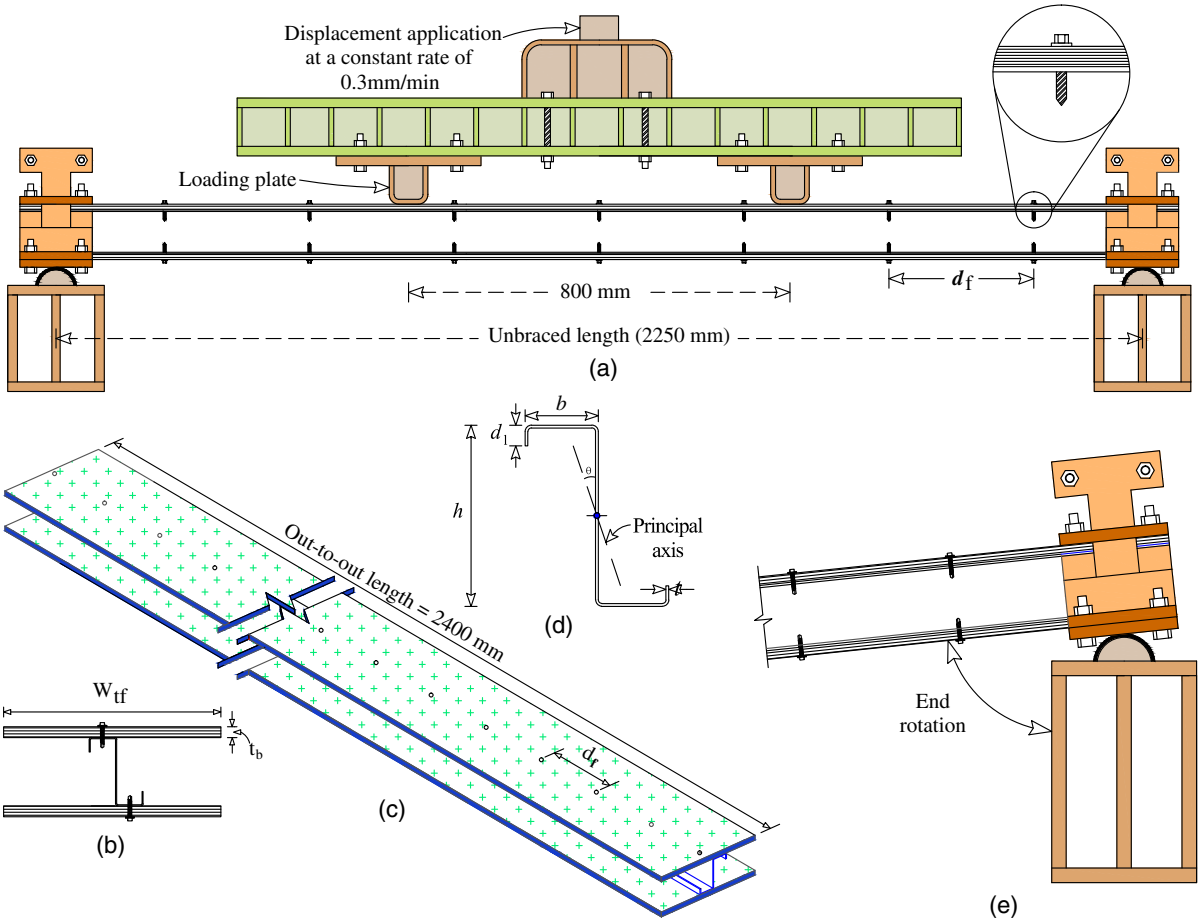

Fig. 4. Experimental test setup: (a) arrangements; (b) identical sheathing-fastener arrangements–crosssectional view of the CFS panel; (c) view of the sheathed CFS panel; (d) cross section of the point-symmetric CFS stud; and (e) end-support arrangements to simulate the simple support conditions.

appropriateness of the support conditions can be verified by comparing the theoretical and experimental stiffness (load-displacement curve). However, it was observed during the experiments that the particle cement board sheathing has broken or separated (pull-through) from the CFS stud [Fig. 6(c)]. Therefore, there is a possibility that the midspan measurements obtained from the experiments are inaccurate. Hence, the applied out-of-plane deflection was used to determine the experimental fastener connection stiffness. The theoretical and experimental moment-deflection of the sheathed CFS wall panel is shown in Fig. 6(a), and it indicates that the test setup arrangements resemble the simple support conditions.

Discussion of Experimental Results: Contribution of PCB Sheathing

In general, the test results show that the PCB-fastener connection has improved the structural performance of the point-symmetric CFS wall studs by transforming the failure mode from biaxial bending to yielding or local buckling (Figs. 6–10). This transformation of the failure mode from unsheathed to sheathed CFS stud has substantially increased the bending moment of the CFS wall stud with a range of 72%–743% (Table 5). The results of the sheathed panels were presented in the form of a moment versus deflection plot as shown in Figs. 6–10 in a direct comparison with calculated design moment capacities (*My*, *M* Sheathed and *M* Unsheathed) for more clarity. The term *My* is the yield moment capacity of the CFS stud cross section calculated by multiplying the elastic section modulus (*Sx*) and yield stress (f_y); *M* Sheathed is the moment capacity of the sheathed CFS stud calculated using the AISI design method with sheathing stiffness combinations (k_y and k_ϕ); and *M* Unsheathed is the design strength of the CFS stud obtained from the direct strength method of AISI. Further, it should be noted that each moment versus deflection plot has four curves corresponding to each specimen as the label implies (e.g., ZL01-12-300).

The increase in bending moment capacity has a good trend against the global slenderness (λ_e) of the point-symmetric CFS stud. The structural contribution of the PCB-fastener connection increases as the global slenderness (λ_e) increases or in other words, the bracing effect of the PCB sheathing remains constant but rather the instability of the point-symmetric CFS stud varies because of it appears that the bracing effect of the sheathing is substantial for the highly slender CFS wall studs. Therefore, it requires more detailed analytical investigation before arriving at definite conclusions. Although, the magnitude of geometric imperfection is high in the CFS slender sections (Selvaraj and Madhavan 2018a), it should be noted that the effect of geometric imperfection on the strength and stiffness of the CFS wall panels was subdued by the substantial bracing effect of sheathing board and hence the individual effect of geometric imperfections could not be captured. In addition, the experimental results indicate that the structural contribution of the sheathing also depends on the PCB-fastener configuration

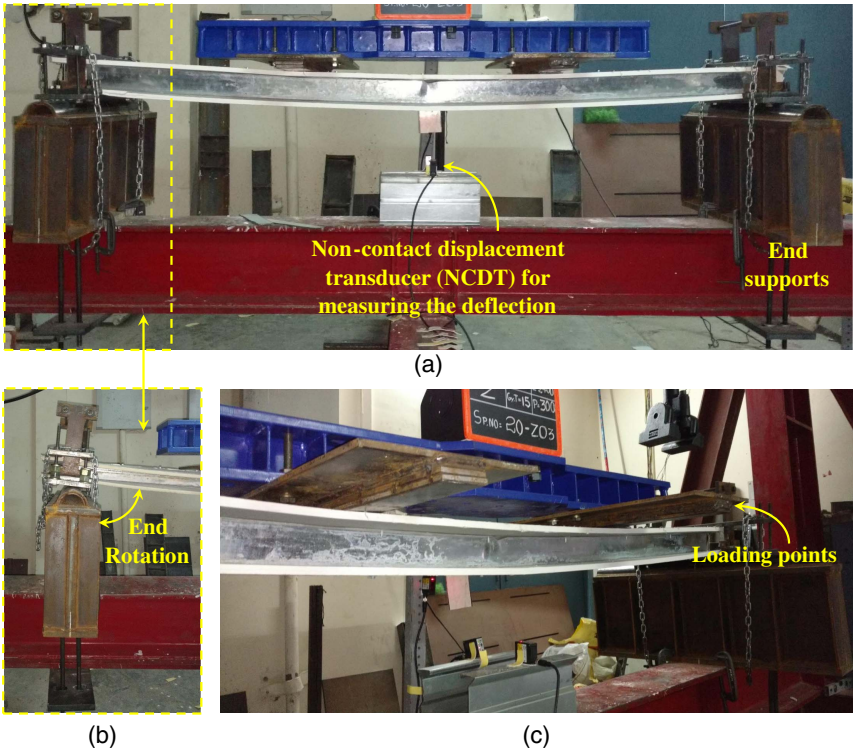

Fig. 5. (a) Actual view of the test setup; (b) end constraint of the supports; and (c) view of the loading points.

(t_b and d_f) as 8 mm thick PCB sheathing board failed in resisting biaxial bending [Figs. 8(c) and 9(c)], whereas 12-mm thick sheathing has inhibited the biaxial bending [Figs. 8(e) and 9(d)].

The AISI 2016 specification was used to determine the design strength of the unsheathed point-symmetric CFS stud. As designed ($\lambda_e \gg 1$), the AISI specification predicted that the biaxial bending is the governing failure mode for unsheathed point-symmetric (Z-shaped) CFS wall studs. The bracing effect of PCB sheathing hindered the biaxial bending in 14 of 20 sheathed studs (Table 5) and in addition 10 of 20 sheathed CFS studs reached the yield moment capacity (M_y = section modulus multiplied by yield stress). This hindering effect by PCB sheathing is in direct contrast to the conclusions of Selvaraj and Madhavan (2018c) where it was concluded that sheathing boards made of powdery composition such as gypsum could not prevent the instability failure modes of CFS studs. The PCB sheathing is also a soft sheathing made of powdery materials with a tensile modulus of 2,548 MPa (Table 4) which is almost equal to the tensile modulus of the gypsum board (2,100 MPa). Therefore, the contradicting results may be attributed to the geometric shape of the CFS stud, which is responsible for the failure modes of the unsheathed CFS studs. It should be noted that the conclusions by Selvaraj and Madhavan (2018b, c) are based on the experiments carried out on singly-symmetric CFS studs (C channels) whereas the present results are based on the point-symmetric CFS studs. This indicates that the sheathing braced design of CFS wall studs should be modified with respect to the failure modes rather than simply based on the bracing ability of the sheathing board, or the fastener connection stiffness predictor equations should have a parameter that represents the geometry of the CFS wall stud.

As the test results indicated that the bracing effect of the sheathing is based on the geometric shape and global slenderness of the CFS stud, the implicit suggestions of the AISI S240 (AISI 2015) to provide hard sheathing with higher modulus or stiffness to brace the CFS stud from global instability can be updated as follows, "the continuous bracing system shall be designed based on the slenderness of the CFS stud."

Design Predictions for PCB Sheathed CFS Wall Studs

Though the structural contribution of the two-sided particle cement board was explored from the experimental results, it is necessary to assess the bracing effect of sheathing in terms of design predictions to verify the suitability of the modified sheathing braced design method. The present study adopts the modified sheathing braced design with fastener connection stiffnesses k_y and k_ϕ proposed by Selvaraj and Madhavan (2018b) [Fig. 2(b)] for sheathed CFS panels subjected to out of plane loading. The modified design method proposed by Selvaraj and Madhavan (2018b) ignores the lateral translational sheathing stiffness (k_x) among the three sheathing stiffnesses suggested by AISI (k_x, k_y, and k_ϕ). his is because the k_x was obtained by applying a shear force at the sheathing-fastener connections (Table 1) and results in an exaggerated sheathing-fastener connections effect at the CFS studs. Although the step by step design procedure of this design concept is explained with model design calculations in Selvaraj and Madhavan (2018b, 2019j), a brief description is given herein as follows: the first task is to determine the fastener connection stiffnesses k_y and k_ϕ using Eqs. (1)–(8) followed by elastic buckling analysis to determine the critical elastic buckling stresses (F_{crl}, F_{cre}, and F_{crd}) using CUFSM software. The final task is to determine the slendernesses of the CFS section (λ_l, λ_d, and λ_e) using F_{crl}, F_{cre}, and F_{crd} and incorporate the slenderness into the design expressions of the direct strength method [Eqs. (7)–(15)].

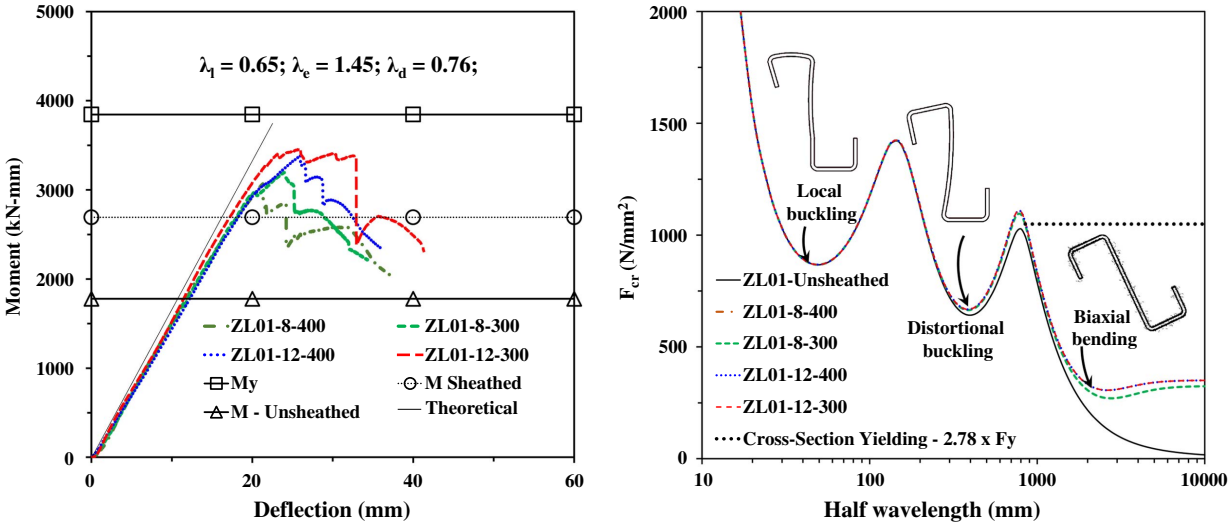

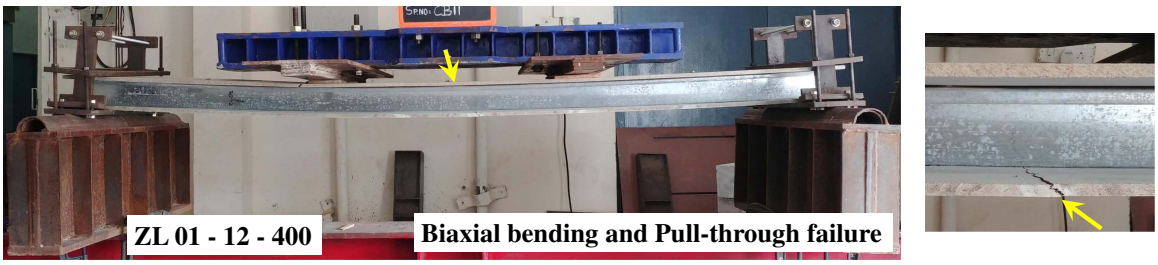

Fig. 6. Test results for ZL01 specimen: (a) moment-displacement plot; (b) buckling curve obtained from CUFSM; and (c–f) failure modes of the sheathing-fastener connections.

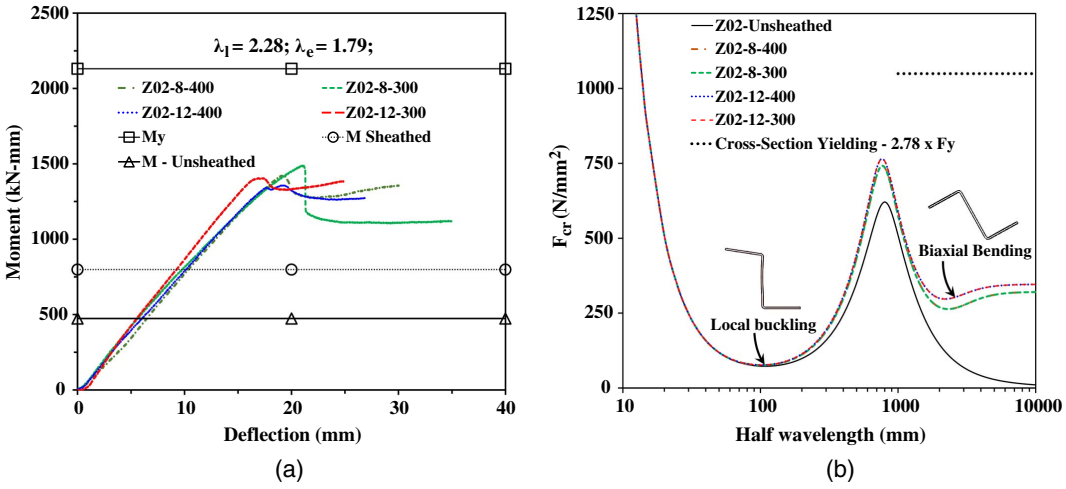

(c)

(d)

(e)

(f)

Fig. 7. Test results for Z02 specimen: (a) moment-displacement plot; (b) buckling curve obtained from CUFSM; and (c–f) failure modes of the sheathing-fastener connections.

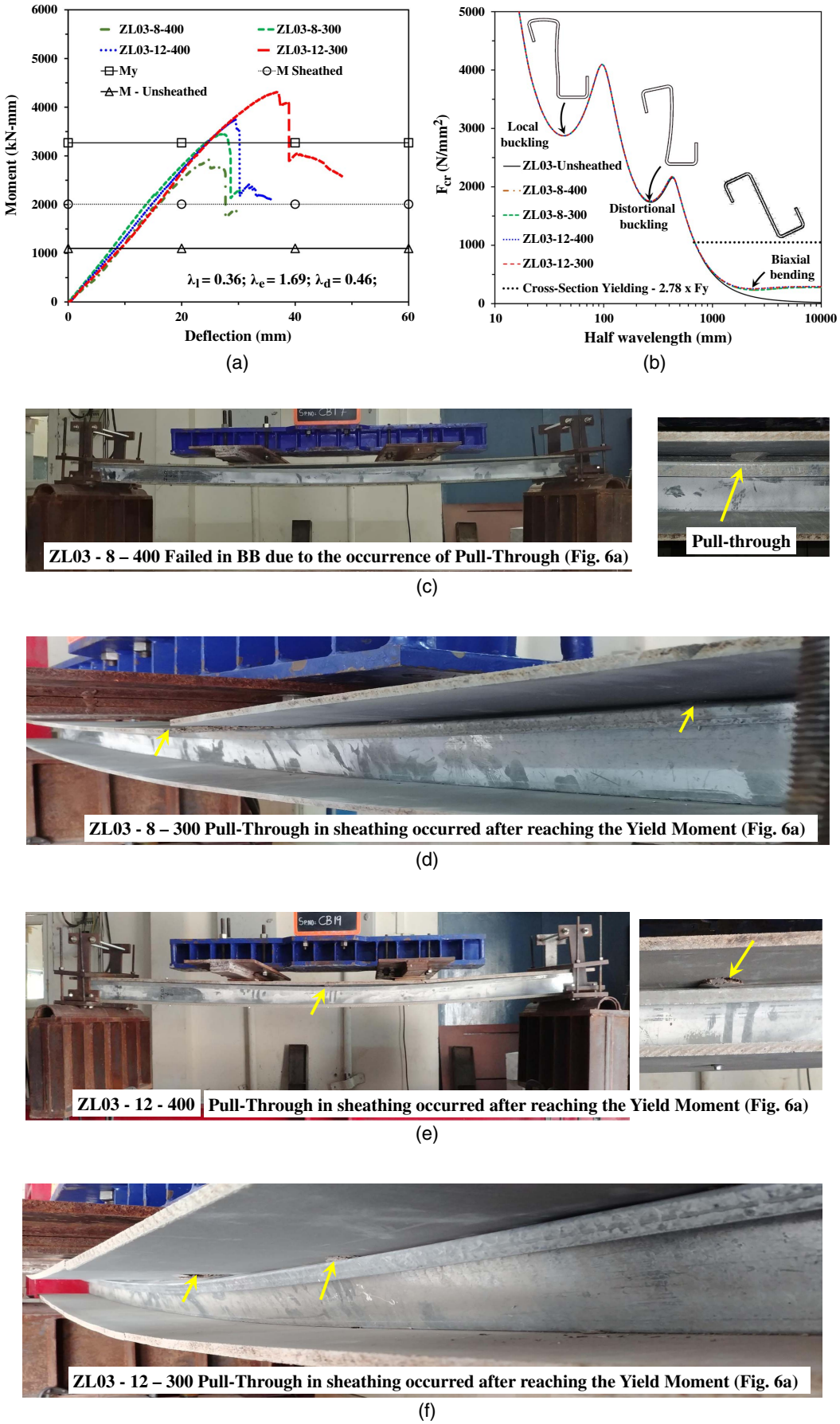

Fig. 8. Test results for ZL03 specimen: (a) moment-displacement plot; (b) buckling curve obtained from CUFSM; and (c–f) failure modes of the sheathing-fastener connections.

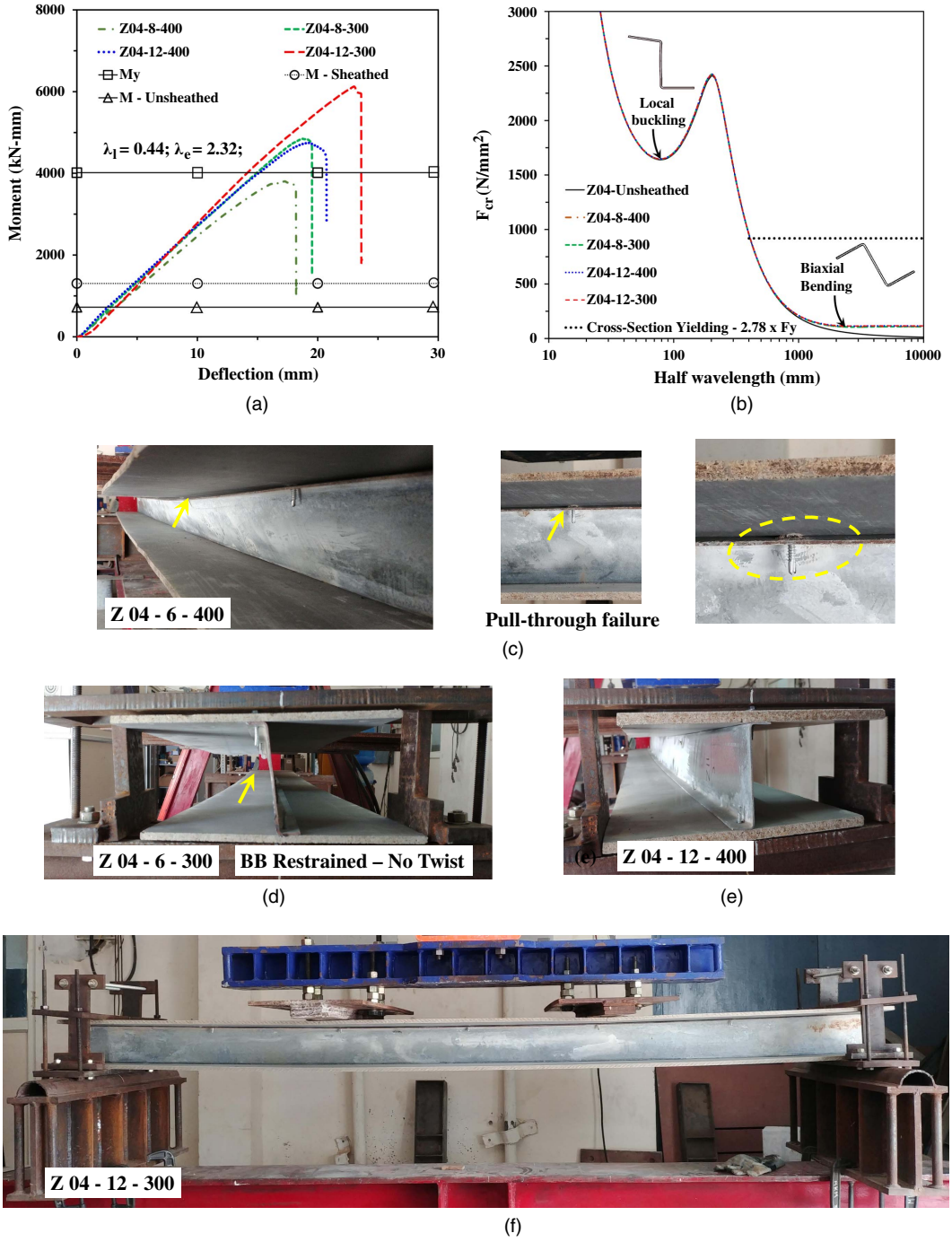

Fig. 9. Test results for Z04 specimen: (a) moment-displacement plot; (b) buckling curve obtained from CUFSM; and (c–f) failure modes of the sheathing-fastener connections.

Determination of Fastener Connection Stiffness

The definition of fastener connection stiffnesses that are present at PCB-fastener connections as per AISI (2013) is given in Table 1. The fastener connection stiffness predictor expressions with descriptions are as follows.

The out-of-plane translational stiffness (k_y), that is acting in the direction of the strong axis (I_{xx}) bending (added flexural stiffness), can be considered in the following ways, assuming (1) no composite action (k_y); (2) partial composite action (k_{yp}) (requires a bending test of the wall panel); and (3) full composite action (k_{yf}) (by simply adding the flexural stiffness of the PCB to the CFS stud). However, the previous investigation by Selvaraj and Madhavan (2018b, c) recommended using the full-composite action for k_y stiffness calculation as it is simple and found to be appropriate, thus, the present study adopts the same

$$k = \frac{(EI)_{fc}\pi^4 d_f}{L^4} \tag{1}$$

$$(EI)_{fc} = (EI)_w + E_g w_{tf} t_b \left(\frac{1}{2}h + \frac{1}{2}t_b\right)^2 \tag{2}$$

where $(EI)_w$ = effective stiffness of the PCB determined from moment of inertia and tensile modulus; L and h = unbraced length and

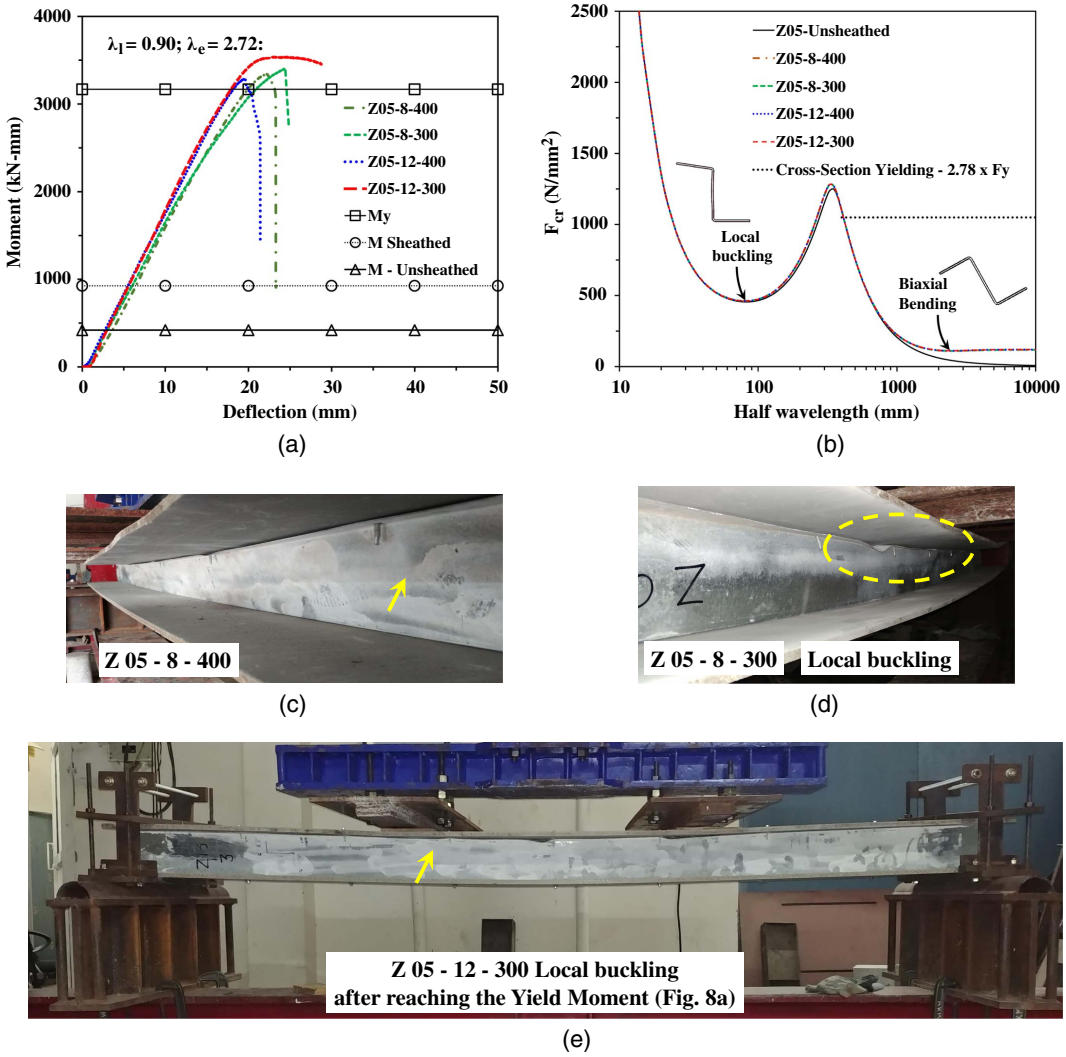

Fig. 10. Test results for Z05 specimen: (a) moment-displacement plot; (b) buckling curve obtained from CUFSM; and (c–e) failure modes of the sheathing-fastener connections.

depth of the CFS stud, respectively; and E_g = tensile modulus of the PCB sheathing. Though a good consistency was observed from the tensile test results of the PCB sheathing board (Table 4), the minimum value of the tensile modulus was used in the calculations of the fastener connection stiffness (Selvaraj and Madhavan 2018c).

The fastener connection stiffness that is acting against the twisting of the CFS cross section is rotational stiffness, k_ϕ. The k_ϕ has two separate sheathing stiffness components, namely localized stiffness provided by the thickness of the CFS stud to the fastener ($k_{\phi c}$) [Eq. (6)] and rotational restraint of the sheathing ($k_{\phi w}$) [Eq. (5)]. The magnitude of rotational sheathing stiffness can be determined from the following equations with respect to the sheathing configurations (thickness and fastener spacing):

$$k_\phi = \underline{k}_\phi d_f \tag{3}$$

$$\underline{k}_\phi = \frac{1}{\underline{k}_{\phi c}} + \frac{1}{\underline{k}_{\phi w}} \tag{4}$$

$$\underline{k}_{\phi w} = \frac{2EI_w}{d_f} \tag{5}$$

$$\underline{k}_{\phi c} = 0.00035E_s t^2 + 75 \tag{6}$$

where E_s and t = Young's modulus and thickness of the CFS stud in the units of lb-f/in.^{2} and in., respectively. The equation [Eq. (6)] for finding the localized stiffness ($k_{\phi c}$) was suggested by Schafer et al. (2011).

Determination of Critical Elastic Buckling Stresses with Sheathing Effect

The next step after the calculation of theoretical fastener-connection stiffness is the determination of critical elastic buckling stresses (F_{crl}, F_{crd}, and F_{cre}) from elastic buckling analysis. The finite strip analysis software *CUFSM* (Li and Schafer 2010) was used for the elastic buckling analysis. The necessity of this finite strip analysis software tool is that the identification of the various buckling modes of the CFS cross sections becomes a simple task. Moreover, the *CUFSM* has an additional option to include the stiffness of the fastener connection (k_y and k_ϕ) in the design. Because the software tool is a two-dimensional one (based on the CFS cross section), the theoretical localized stiffnesses (k_y, and k_ϕ) are converted as stiffness per unit length, therefore, the stiffnesses k_y, and k_ϕ are divided by the fastener spacing (d_f). Hence, these stiffness

Table 5. Comparison of moment capacities (sheathed panel results): Experiment versus prediction

Panel ID	Moment (M-unsheathed) (kN mm)	Experiment			Improved strength M-unsheathed versus M_{EXP} (%)
		Moment (M_{EXP}) (kN mm)	Failure mode		
			CFS Stud	Sheathing	
ZL01-8-400	1,778.3	3,067.4	BB	Pull-through	72.5
ZL01-8-300		3,196.6	BB	Pull-through	79.8
ZL01-12-400		3,381.1	BB	Pull-through	90.1
ZL01-12-300		3,458.7	BB	Pull-through	94.5
Z02-8-400	474	1,421.1	LB	No failure	199.8
Z02-8-300		1,490.2	LB	No failure	214.4
Z02-12-400		1,358.6	LB	No failure	186.6
Z02-12-300		1,405.5	LB	No failure	196.5
ZL03-8-400	1,100.5	2,927.9	BB	Pull-through	166.1
ZL03-8-300		3,444.0	Y	Pull-through[a]	213.0
ZL03-12-400		3,744.7	Y	Pull-through[a]	240.3
ZL03-12-300		4,314.6	Y	Pull-through[a]	292.1
Z04-8-400	724.1	3,802.3	BB	Pull-through	425.1
Z04-8-300		4,845.4	Y	Pull-through[a]	569.2
Z04-12-400		4,742.7	Y	Pull-through[a]	555.0
Z04-12-300		6,126.7	Y	Pull-through[a]	746.1
Z05-8-400	419.5	3,341.4	Y	No failure	696.5
Z05-8-300		3,405.5	Y	No failure	711.7
Z05-12-400		3,284.1	Y	No failure	682.8
Z05-12-300		3,536.8	Y	No failure	743.0

Note: LB = local buckling; BB = biaxial buckling; Y = yielding failure; M_{EXP} = experimental strength; and M-unsheathed = unsheathed design strength.
[a]Specimens failed in pull-through after achieving the yield moment capacity.

magnitudes per unit length may be noted with an underline as k_y, and k_ϕ. The determined fastener connection stiffnesses per unit length with respect to the sheathing configurations (t_b and d_f) and CFS stud type are summarized in Table 6. The calculated stiffnesses from Table 6 are included in the CFS stud model at the location of sheathing-fastener connections (midpoint node of the bottom and top flange) as shown in Fig. 11. The elastic buckling analysis results are presented in the form of buckling curves in Figs. 6(b), 7(b), 8(b), 9(b), and 10(b), respectively for each CFS wall panel set.

In general, the *CUFSM* analysis results show that the biaxial bending moment ($M_{cre} = S_f \times F_{cre}$) of the CFS wall studs have been improved after incorporating the fastener-connection stiffnesses (k_y and k_ϕ) as shown in Table 6 and elastic buckling analysis curves obtained from *CUFSM* version 4.03 software [Figs. 6(b), 7(b), 8(b), 9(b), and 10(b)]. Although there is a considerable improvement in global buckling strength, no CFS stud has reached the yield moment capacity (M_y) with the presence of the fastener connection stiffnesses whereas the experimental results indicate that 10 of 20 CFS panels have reached the yield moment capacity [lines with legend M_y in Figs. 6(a), 7(a), 8(a), 9(a), and 10(a)] because of the structural contribution of sheathing. According to AISI S100, the biaxial bending critical elastic buckling stress should be higher than 2.78 times the yield stress (f_y) in order to be considered as having attained yield moment capacity [dotted line with a legend "Cross-Section Yielding–$2.78 \times F_y$" in Figs. 6(b), 7(b), 8(b), 9(b), and 10(b)]; however, no global buckling curve has reached the limit of 2.78 time yield stress. This indicates that the elastic buckling analysis results should not be compared with the experimental results. Further, the elastic buckling analysis results also show that the critical elastic buckling stresses of the local and distortional modes are not influenced by the contribution of fastener-connection stiffnesses ($\underline{k}_y$ and $\underline{k}_\phi$). The noninfluence of sheathing stiffness on the local and distortional buckling could be because of the sheathing stiffnesses k_y and k_ϕ were arrived at for global bending and torsional resistance only (Vieira and Schafer 2012a). These unmatched elastic buckling results with respect to the corresponding experimental results necessitate more detailed discussion on predicted moment capacity by the direct strength method, which is described in the following sections.

Direct Strength Method Design Expressions

The DSM design expressions for beam design from section F of AISI S100-16 (AISI 2016) are summarized herein. The unfactored design moment or the nominal moment capacity of the beam member (M_{DSM}) is the minimum nominal moment for local buckling (M_{nl}), distortional buckling (M_{nd}), and biaxial bending (M_{ne}), as shown in Eq. (7). In addition, AISI (2016) suggests taking advantage of inelastic buckling strength for local and distortional buckling in the design strength if the beam is adequately braced from biaxial bending by steel bracing or continuous sheathing [Eqs. (10) and (12)]

$$M_{DSM} = \min(M_{ne}, M_{nl} \text{ and } M_{nd}) \tag{7}$$

Local buckling strength (M_{nl})

$$M_{nl} = M_{ne} \quad \text{for } \lambda_l \le 0.776 \tag{8}$$

$$M_{nl} = M_y + \left(1 - \frac{1}{C_{yl}^2}\right)(M_p - M_y) \quad \text{for } \lambda_l \le 0.776 \quad \text{and} \quad M_{ne} \ge M_y \tag{9}$$

Table 6. Comparison of moment capacities (sheathed panel results): Experiment versus prediction

Panel ID	Sheathing configuration: Sheathing thickness	Sheathing configuration: Fastener spacing	k_y (N/mm/mm) Eqs. (1)–(2)	k_ϕ (N · mm/mm/rad) Eqs. (3)–(6)	Elastic buckling analysis results: M_{crl}/M_y	M_{crd}/M_y	M_{cre}/M_y
ZL01-Un	Unsheathed		—	—	2.30	1.70	0.46
ZL01-8-400	8	400	0.048	104.5	2.30	1.76	0.75
ZL01-8-300	8	300	0.048	104.5	2.30	1.76	0.75
ZL01-12-400	12	400	0.078	110.1	2.30	1.77	0.81
ZL01-12-300	12	300	0.078	110.1	2.30	1.77	0.81
Z02-Un	Unsheathed		—	—	0.19	—	0.31
Z02-8-400	8	8	0.044	86.3	0.20	—	0.70
Z02-8-300	8	8	0.044	86.3	0.20	—	0.70
Z02-12-400	12	12	0.071	90.0	0.20	—	0.79
Z02-12-300	12	12	0.071	90.0	0.20	—	0.79
ZL03-Un	Unsheathed		—	—	7.62	4.60	0.34
ZL03-8-400	8	8	0.038	129.3	7.62	4.65	0.62
ZL03-8-300	8	8	0.038	129.3	7.62	4.65	0.62
ZL03-12-400	12	12	0.062	137.8	7.62	4.66	0.68
ZL03-12-300	12	12	0.062	137.8	7.62	4.66	0.68
Z04-Un	Unsheathed		—	—	4.96	—	0.18
Z04-8-400	8	8	0.072	163.0	4.98	—	0.32
Z04-8-300	8	8	0.072	163.0	4.96	—	0.32
Z04-12-400	12	12	0.116	176.8	4.99	—	0.35
Z04-12-300	12	12	0.116	176.8	4.96	—	0.35
Z05-Un	Unsheathed		—	—	1.21	—	0.13
Z05-8-400	8	8	0.077	104.5	1.22	—	0.29
Z05-8-300	8	8	0.077	104.5	1.22	—	0.29
Z05-12-400	12	12	0.123	110.1	1.22	—	0.30
Z05-12-300	12	12	0.123	110.1	1.22	—	0.30

Note: M_{crd} = critical elastic distortional buckling moment; M_{cre} = critical elastic lateral torsional buckling moment; M_{crl} = critical elastic local buckling moment; and M_y = yield moment;

$$M_{nl} = \left[1 - 0.15\left(\frac{M_{crl}}{M_y}\right)^{0.4}\right]\left(\frac{M_{crl}}{M_y}\right)^{0.4} M_y \quad \text{for } \lambda_l > 0.776 \tag{10}$$

Distortional buckling strength (M_{nd})

$$M_{nd} = M_y + \left(1 - \frac{1}{C_{yd}^2}\right)(M_p - M_y) \quad \text{for } \lambda_d \le 0.673 \tag{11}$$

$$M_{nd} = \left[1 - 0.22\left(\frac{M_{cd}}{M_y}\right)^{0.5}\right]\left(\frac{M_{crd}}{M_y}\right)^{0.5} M_y \quad \text{for } \lambda_d > 0.673 \tag{12}$$

Lateral-torsional buckling strength (M_{ne})

$$M_{ne} = M_{cre} \quad \text{for } M_{cre} < 0.56M_y \tag{13}$$

$$M_{ne} = \frac{10}{9} M_y \left(1 - \frac{10M_y}{36M_{cre}}\right) \quad \text{for } 2.78M_y \ge M_{cre} \ge 0.56M_y \tag{14}$$

$$M_{ne} = M_y \quad \text{for } M_{cre} > 2.78M_y \tag{15}$$

where M_y = yield moment capacity of the beam; $M_y = S_f f_y$; f_y = yield stress from coupon tests; S_f = gross elastic section modulus; $\lambda_l = \sqrt{(M_y/M_{crl})}$; M_{crl} = critical elastic moment for local buckling; $M_{crl} = S_f f_{crl}$; $C_{yl} = \sqrt{(0.776/\lambda_l)} \le 3$; $\lambda_d = \sqrt{(M_y/M_{crd})}$; $M_{crd} = S_f f_{crd}$; M_{crd} = critical elastic moment for distortional buckling; $C_{yd} = \sqrt{(0.673/\lambda_d)} \le 3$; $M_{cre} = S_f f_{cre}$; M_{cre} = critical elastic moment for biaxial bending; M_p = member plastic moment; $M_p = Z_f f_y$; Z_f = plastic section modulus; f_{crl}, f_{crd}, and f_{cre} are the critical elastic buckling stresses obtained either from *CUFSM* (Li and Schafer 2010) for sheathed member or *Thinwall* (Papangelis and Hancock 1995) for local (F_{crl}), distortional (F_{crd}), and biaxial bending (F_{cre}), respectively.

Design Results

Overall, the comparison between the experimental moment (M_{EXP}) and predicted moment capacities indicates that the design results are overly conservative as shown in Table 7 (mean $M_{EXP}/M_{Sheathed} = 2.38$). In addition, the design test results show that the structural contribution of the PCB has increased the design moment capacity of the sheathed wall panel by 51%–124% compared to the unsheathed CFS studs moment capacity ($M_{Unsheathed}$). Although, this percentage of improvement is much less compared to the experimentally observed ones ($M_{EXP}/M_{Unsheathed}$), the trend of increase in moment capacity ($M_{Sheathed}$ versus $M_{Unsheathed}$) matches the trend observed from the experimental results (M_{EXP} versus $M_{Unsheathed}$), i.e., "the bracing effect of sheathing increases as the slenderness of the CFS stud increases." In addition, the reliability study was also carried out to assess the suitability of the sheathing braced design method used (with k_y and k_ϕ).

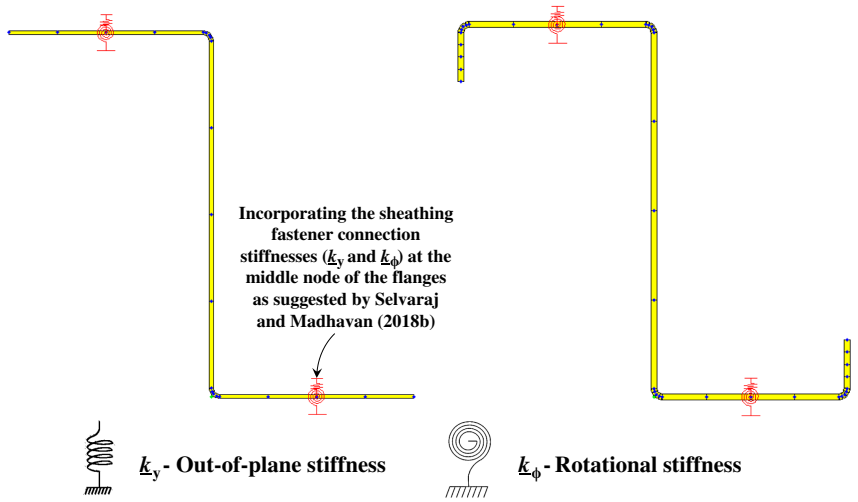

Fig. 11. Elastic buckling analysis models for sheathed CFS panels subjected to out-of-plane loading according to Selvaraj and Madhavan (2018b).

Table 7. Comparison of moment capacities (sheathed panel results): Experiment versus prediction

Panel ID	Design predictions: Moment (M-sheathed) (kN mm) Eqs. (7)–(15)	Design predictions: Failure mode (gov.)	Improved strength M sheathed versus M-unsheathed	Comparison M_{EXP}/M-sheathed
ZL01-Un	1,778.3	—	—	—
ZL01-8-400	2.6916	BB	51.4	1.14
ZL01-8-300	2.6916	BB		1.19
ZL01-12-400	2.8093	BB	58	1.20
ZL01-12-300	2.8093	BB		1.23
Z02-Un	474	—	—	—
Z02-8-400	0.7985	LB	68.4	1.78
Z02-8-300	0.7985	LB		1.87
Z02-12-400	0.8358	LB	76.3	1.63
Z02-12-300	0.8358	LB		1.68
ZL03-Un	1100.5	—	—	—
ZL03-8-400	2.0077	BB	82.4	1.46
ZL03-8-300	2.0077	BB		1.72
ZL03-12-400	2.1417	BB	94.6	1.75
ZL03-12-300	2.1417	BB		2.01
Z04-Un	724.1	—	—	—
Z04-8-400	1.3048	BB	80.2	2.91
Z04-8-300	1.3048	BB		3.71
Z04-12-400	1.3916	BB	92.2	3.41
Z04-12-300	1.3916	BB		4.40
Z05-Un	419.5	—	—	—
Z05-8-400	0.9251	BB	120.5	3.61
Z05-8-300	0.9251	BB		3.68
Z05-12-400	0.9398	BB	124.0	3.49
Z05-12-300	0.9398	BB		3.76
Mean (P_m)				2.38
Coefficient of variation (V_p)				0.459
Reliability index (ASCE 2010) (β_1)				2.94
Reliability index (AS/NZS 2002) (β_2)				2.94

Note: $M_{Sheathed}$ = Sheathed design strength.

The reliability index values (β_1 and β_2) were calculated for two different load combinations specified in the commonly used design standards: β_1 corresponds to the load combination 1.2 dead load (DL) + 1.6 live load (LL) as specified in the ASCE standard (ASCE 2010) and β_2 corresponds to the load combination 1.25DL + 1.5LL as specified in the Australian/New Zealand standard (AS/NZS 2002). The reliability index values for the obtained results ($M_{EXP}/M_{Sheathed}$, Table 7) indicate that the design method used is suitable [β_1 and β_2 are higher than the target reliability index value 2.5 per AISI (2016) and Wang and Young (2015)]. However, the large variation between the predicted and experimental values (mean $M_{EXP}/M_{Sheathed} = 2.38$) will be investigated while assessing the appropriateness of the design method. The large difference between the experimental (M_{EXP}) and predicted moment

capacities by use of modified sheathing braced design method (M_{Sheathed}) may be because of the following theoretical and practical facts:

1. The overly conservative moment capacity (M_{Sheathed}) predictions by the design equations are predominantly because of the inaccurate failure mode predictions. It can be observed from the moment versus deflection plots [Figs. 6(a), 7(a), 8(a), 9(a), and 10(a)] and Table 7 that the failure modes predicted using modified sheathing braced design method are inaccurate for 10 of 20 specimens tested. This should be because of the fact that the localized sheathing stiffness predictor expressions do not take in to consideration the shape and geometric property of the CFS stud.
2. The particle cement board practically restrains the waviness of the local buckling by leaning on the flanges of the CFS stud. This preventive effect of PCB sheathing can be observed from Figs. 7(c–f) and 10(c–e). The similar restraining effect of sheathing was observed by Wang et al. (2019a, b) in concrete infilled steel columns. However, this practical effect was not incorporated in the DSM expressions [Eqs. (7)–(15)], thus the experimental results are significantly higher than the design moment predictions.
3. Although the structural contribution of the PCB sheathing on local buckling capacity of the CFS stud was observed in experimental results, this was not captured in the elastic buckling analysis as shown in Figs. 6(b), 7(b), 8(b), 9(b), and 10(b) and Table 6 (M_{crl}/M_y and M_{crd}/M_y sheathed versus unsheathed in the same set of specimens). This inaccuracy in the failure mode prediction could be because of the incorrect input to the elastic buckling analysis, i.e., the variables of the fastener connection stiffness predictor expressions.
4. In general, the DSM expressions are overly conservative for the CFS members with higher instability [AISI S100 (AISI 2016); Schafer 2006; Selvaraj and Madhavan 2019m].

Further investigation on the design calculations indicates that the current fastener connection stiffness (localized) predictor expressions [Eqs. (1)–(6)] are derived from the single experimental test setup and single CFS stud type but was proposed for all design applications. The magnitudes of the rotational sheathing stiffness per unit length (k_ϕ) are identical for the CFS studs ZL01 and Z05 (Table 6), even though there is a large difference between the global slenderness (λ_e) magnitudes (Table 3). This is because Eqs. (3)–(6), used to determine the localized sheathing bracing stiffness, are primarily based on the CFS stud thickness (t). It is improper to have equal fastener-connection stiffness magnitudes for the CFS structural members with different geometry that induce the failure modes, such as slenderness (λ_l, λ_d, and λ_e), moment of inertia (I_{xx} and I_{yy}), and torsional constant (J). Previous studies on torsional buckling of the steel beams indicate: (1) the global slenderness of the singly symmetric cross-section significantly influences the rate of cross-sectional twist (Madhavan et al. 2015; Selvaraj et al. 2016; Selvaraj and Madhavan 2016, 2017a, b; h; k, c, g); and (2) the failure mode of CFS studs also vary depending on the cross-section geometry (singly, doubly, and point–symmetric) and loading conditions. The singly, point, and doubly symmetric CFS sections failure modes are lateral-torsional buckling (combination of lateral and vertical displacement), biaxial bending (rotation about longitudinal axis), and lateral buckling (lateral movement only), respectively. Therefore, it is necessary that future investigations of sheathing braced design of CFS studs should focus on developing a robust design expression by considering all the previously mentioned points. To further endorse the previous conclusions and suggestions pertaining to the predicted moment capacities (M_{Sheathed}) and failure modes using the modified sheathing braced design method with the fastener-connection expressions [Eqs. (1)–(6)], the fastener connection strength and fastener spacing demand check were carried out in

Table 8. Check for fastener spacing

Panel ID	Sheathing thickness (t_b) (mm)	Fastener spacing (d_f) (mm)	T_r (N mm)		$f_{r\text{-}pt}$ (N) [Eq. (16)]		$P_{n\text{-}pt}$ (N) $\phi = 0.5$	Comparison $P_{n\text{-}pt}/f_{r\text{-}pt}$		Check for sheathing configuration $P_{n\text{-}pt}$ versus $f_{r\text{-}pt}$
			UDL	Three point load	UDL	Three point load		UDL	Three point load	
ZL01-8-400	8	400	49,228.2	41,536.3	31.44	26.53	88.96	2.83	3.35	The theoretical check indicates that the ($f_{r\text{-}pt} < P_{n\text{-}pt}$) strength of the sheathing-fastener connection is sufficient to arrest the pull-through failure at the sheathing-fastener connection.
ZL01-8-300		300	36,921.2	41,536.3	20.08	22.59		4.43	3.94	
ZL01-12-400	12	400	51,381.0	43,352.7	59.52	50.22		1.49	1.77	
ZL01-12-300		300	38,535.8	43,352.7	36.35	40.89		2.45	2.18	
Z02-8-400	8	400	9,580.0	8,083.1	13.17	11.11		6.76	8.01	
Z02-8-300		300	7,185.0	8,083.1	7.92	8.90		11.24	9.99	
Z02-12-400	12	400	10,028.3	8,461.4	27.36	23.09		3.25	3.85	
Z02-12-300		300	7,521.2	8,461.4	16.31	18.34		5.46	4.85	
ZL03-8-400	8	400	30,484.4	25,721.2	31.08	26.22		2.86	3.39	
ZL03-8-300		300	22,863.3	25,721.2	21.04	23.67		4.23	3.76	
ZL03-12-400	12	400	32,518.1	27,437.2	52.42	44.23		1.70	2.01	
ZL03-12-300		300	24,388.6	27,437.2	33.64	37.85		2.64	2.35	
Z04-8-400	8	400	26,901.4	22,698.0	18.42	15.54		4.83	5.73	
Z04-8-300		300	20,176.0	22,698.0	12.95	14.57		6.87	6.11	
Z04-12-400	12	400	28,690.2	24,207.3	28.14	23.74		3.16	3.75	
Z04-12-300		300	21,517.6	24,207.3	18.84	21.20		4.72	4.20	
Z05-8-400	8	400	15,240.2	12,858.9	10.67	9.01		8.33	9.88	
Z05-8-300		300	11,430.2	12,858.9	6.80	7.66		13.07	11.62	
Z05-12-400	12	400	15,484.0	13,064.6	19.87	16.77		4.48	5.31	
Z05-12-300		300	11,613.0	13,064.6	12.08	13.59		7.36	6.54	
Mean								5.11	5.13	
Minimum								1.49	1.77	
Maximum								13.07	11.62	

Note: $P_{n\text{-}pt}$ = actual strength of sheathing-fastener connection against pull-through failure; and $f_{r\text{-}pt}$ = force demand at each sheathing-fastener connection to avoid pull-through failure. UDL = uniformly distributed load.

the "Check for Sheathing-Fastener Connection Strength Demand" section as per AISI (2013).

Check for Sheathing-Fastener Connection Strength Demand

The purpose of the sheathing-fastener demand calculations is to check the appropriateness of the sheathing configurations in hindering the global instability of the CFS stud. The logic behind the demand check is simple: the fastener connection should be able to restrain the torsion force ($f_{r\text{-}pt}$) developed because of the design load (w_r). The force developed at the fastener connection location can be predicted using the following expression [Eq. (16)] of AISI (2013)

$$f_{r-pt} = \frac{T_r}{b/2}\frac{k_\phi}{2k_\phi + 2k_x(h^2/4)} < P_{n-pt} \tag{16}$$

where f_{r-pt} = force developed; $T_r = w_d d_f e$; w_d = load on the CFS stud; $w_d = 4M/L$ (three–point loading) and $w_d = 8M/L^2$ (UDL); L = unbraced length of the CFS stud; $M = M_{\text{Sheathed}}$; d_f = center–center distance between the two fasteners; e = eccentricity ($e = SC\text{-}t/2 + r_o$); SC = distance between shear center and center line of web; t = stud thickness; r_o = corner radius (usually taken as $2t$); k_x (N/mm) and k_ϕ (N · mm/mm/rad) = fastener connection stiffnesses against the lateral movement and cross-sectional twist (rotation) of the CFS stud, respectively; b = outer-to-outer breadth of flange; h = outer–to–outer depth of web; and P_{n-pt} is the actual strength of the fastener connection against the cross-sectional twist of the CFS stud.

The force (f_{r-pt}) developed because of buckling of the CFS stud was determined using Eq. (16). The actual strength (pull-through) of the fastener connection (P_{n-pt}) against the buckling of the CFS stud is taken as 88.96 N (Vieira and Schafer 2012a, b;

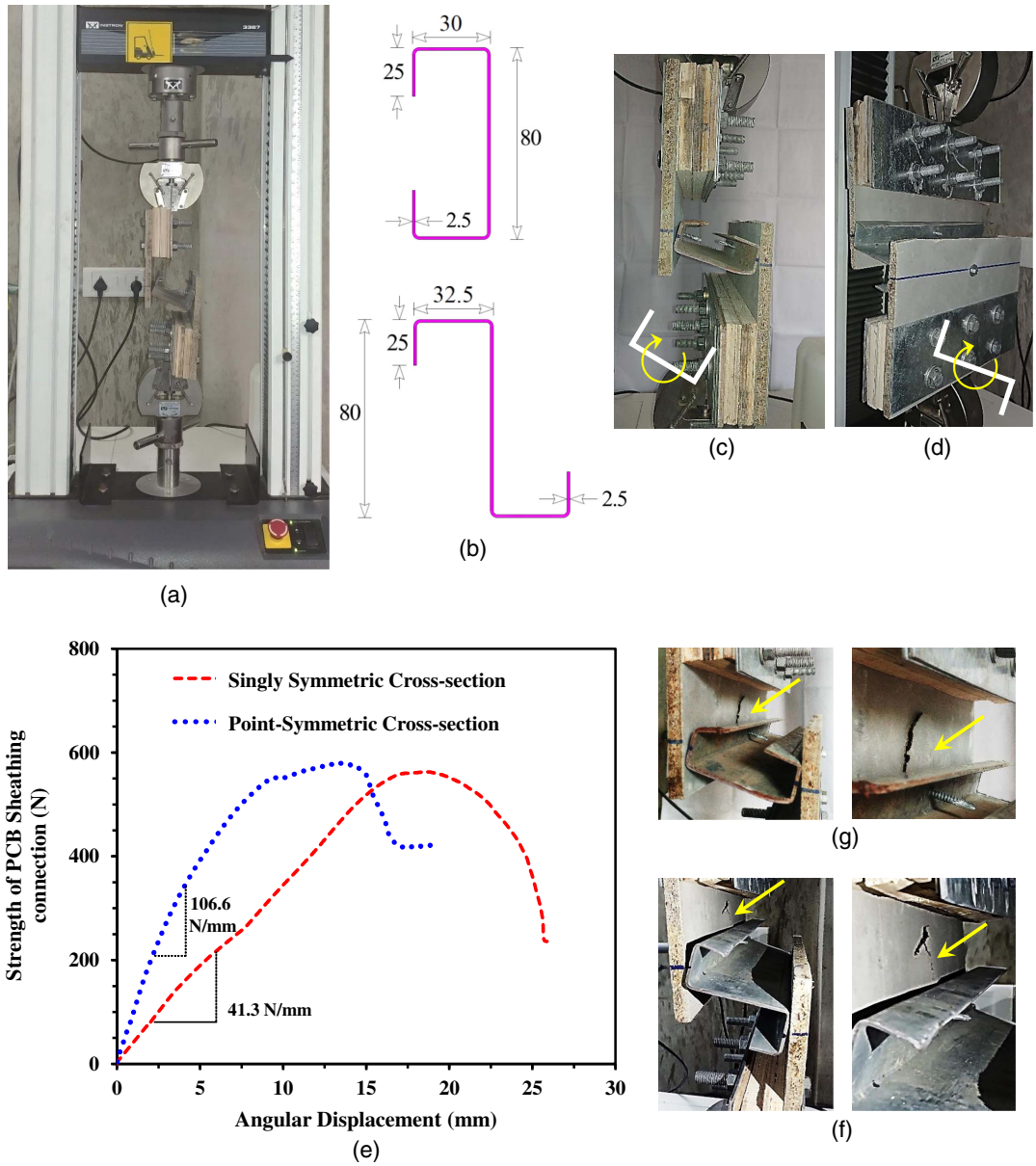

Fig. 12. (a) New test setup proposed by Selvaraj and Madhavan (2019i) to investigate the behavior of sheathing-fastener connections; (b) dimensions of the CFS studs; (c–d) failure mode of the sheathing-fastener connections; (e) sheathing fastener connection strength versus angular displacement of the CFS stud; (f) pull-through failure of the sheathing-fastener connections in singly symmetric CFS studs; and (g) pull-through failure of the sheathing-fastener connections in point symmetric CFS studs.

Peterman and Schafer 2014). The comparison between the actual strength (P_{n-pt}) and force developed (f_{r-pt}) indicates that the sheathing configuration provided is sufficient ($P_{n-pt} > f_{r-pt}$) to inhibit the cross-sectional twist of the CFS studs (Table 8). However, this ability of sheathing-fastener connection was not reflected in the full-scale experiments as 6 of the 20 CFS wall studs failed in biaxial bending because of the pull-through failure of PCB sheathing. Therefore, the incorrect strength demand predictions by AISI (2013) may be attributed to the inadequacy of the AISI equations [k_x and k_ϕ] in predicting the stiffness of sheathing-fastener connection. Further revision is essential to precisely design the required sheathing-fastener connections to brace the CFS wall stud.

Design Guidelines for Sheathing-Fastener Connections

As it was demonstrated that the current AISI expression for the prediction of fastener connection stiffness is inaccurate, a new test setup was developed to investigate the bracing effect of sheathing in CFS wall panels as shown in Fig. 12(a). The newly proposed test setup was created to accurately simulate the biaxial bending of the CFS stud and induces pull-through failure at the fastener connections. The proposed test setup and the observed failure modes of the fastener connections are shown in Figs. 12(a–d). The tests on sheathing-fastener connections were carried out on both singly-symmetric (C channel) and point-symmetric (Z-shaped) CFS studs with almost similar dimensions [Fig. 12(b)]. However, the stiffness of the 12 mm thick PCB sheathing against the angular displacement of the CFS stud varies significantly as shown in Fig. 12(e). The initial stiffness of the PCB sheathing board is 41.3 N/mm and 106.6 N/mm for singly-symmetric and point-symmetric studs. This significant variation in the stiffness magnitudes may be attributed to the geometric properties of the CFS studs [I_{xx} of singly symmetric and point symmetric is 3.657×10^5 and 4.737×10^5 mm^4, respectively; J of singly symmetric and point symmetric is 898.6 and 924.6 mm^4, respectively]. The test results ratify the hypothesis concluded from the full-scale CFS panel tests that the fastener connection stiffness magnitudes are based on the shape and geometric properties of the CFS stud. Therefore, it is suggested that the current AISI fastener connection stiffness predictor expressions be revised with appropriate design parameters.

Conclusions

The bracing effect of fastener-connection on point-symmetric CFS stud provided at the fastener connection is explored through full-scale experiments. It was found that there is a potential benefit in terms of design strength when the instability failures of the CFS studs are inhibited by the appropriate sheathing-fastener connections. Specifically, the fastener connection with PCB sheathing of thickness 12 mm was able to inhibit the biaxial bending of the CFS studs subjected to out-of-plane loading, thus the strength of the panel increased tremendously by 72%–743% compared to the unsheathed CFS stud. The design moment capacities of the CFS wall panels are determined using the modified design approach with the expressions of AISI. It was observed from the design results that the predicted failure modes varied significantly compared to the experimental failure modes. Further investigation revealed the inability of current AISI expression to predict the fastener connection stiffnesses. The inability is because of the lack of consideration of geometric properties and shape of the CFS stud which influences the strength and stability of the CFS stud. Therefore, a new test setup is proposed to determine the sheathing-fastener connection stiffness. The results from the new sheathing-fastener connection test indicate that the stiffness of the sheathing depends on the shape of the CFS studs. Hence, the current AISI fastener connection stiffness predictor expressions may be modified after further research work with the proposed test setup.

Data Availability Statement

Some or all data, models, or code generated or used during the study are available from the corresponding author by request. The list of data includes (a) the values used for plotting the Fig. (b) Photographs of failure modes of the test specimens.

Notation

The following symbols are used in this paper:

a = fastener spacing in $2a$ rule;
BB = biaxial bending;
b = breadth of flange (out-to-out);
c_b = bending coefficient;
d = diameter of the fastener used in the sheathing-fastener connection;
d_l = depth of the lip in the lipped point-symmetric section;
d_f = fastener spacing;
E_s = Young's modulus of steel (from testing);
E_g = tensile modulus of PCB sheathing (from testing);
e = eccentricity;
f_{crd} = elastic critical distortional buckling stress (obtained from elastic buckling analysis);
f_{cre} = elastic critical lateral torsional buckling stress (obtained from elastic buckling analysis);
f_{crl} = elastic critical local buckling stress (obtained from elastic buckling analysis);
$f_{r\text{-}pt}$ = force demand to resist the pull through failure of sheathing;
f_y = yield stress of the CFS sections obtained from tensile test;
h = depth of web (out-to-out);
k_x = sheathing lateral translational stiffness;
k_y = out of plane (vertical) translational stiffness;
$\underline{k}_y$ = out of plane (vertical) translational foundation stiffness;
k_ϕ = sheathing rotational stiffness;
$\underline{k}_\phi$ = sheathing rotational foundation stiffness;
$k_{\phi c}$ = localized connection stiffness;
$k_{\phi w}$ = sheathing rotational restraint;
L = unbraced length of the CFS stud;
LB = local buckling;
M_{crd} = critical elastic distortional buckling moment ($S_f \cdot f_{cre}$);
M_{cre} = critical elastic lateral torsional buckling moment ($S_f \cdot f_{cre}$);
M_{crl} = critical elastic local buckling moment ($S_f \cdot f_{crl}$);
M_{EXP} = ultimate moment capacities obtained from experimental results;
M_{DSM} = nominal flexural design strength predicted from DSM;

M_{Sheathed} = nominal flexural design strength of the unsheathed CFS stud predicted from DSM;
M_{nd} = nominal flexural strength for distortional buckling;
M_{ne} = nominal flexural strength for lateral torsional buckling;
M_{nl} = nominal flexural strength for local buckling;
M_p = member plastic moment ($Z_f.f_y$);
$M_{\text{Unsheathed}}$ = nominal flexural design strength of the sheathed CFS stud predicted from DSM;
M_y = member yield moment ($S_f.f_y$);
P_{n-pt} = available strength at the fastener-sheathing against pull-through;
S_f = gross elastic section modulus;
T_r = torsion because of the design load;
t = base metal thickness of CFS sections;
t_b = sheathing thickness;
w_{tf} = fastener tributary width;
Z_f = plastic section modulus;
λ_d = section slenderness for distortional buckling $(F_y/F_{crd})^{0.5}$;
λ_e = section slenderness for global buckling $(F_y/F_{cre})^{0.5}$; and
λ_l = section slenderness for local buckling $(F_y/F_{crl})^{0.5}$.

References

AISI (American Iron and Steel Institute). 1983. *Cold-formed steel design manual*. AISI 21. Washington, DC: AISI.

AISI (American Iron and Steel Institute). 1986. *Specification for the design of cold-formed steel structural members*. Washington, DC: AISI.

AISI (American Iron and Steel Institute). 2012. *North American standard for cold-formed steel framing floor and roof system design*. AISI S210-07. Washington, DC: AISI.

AISI (American Iron and Steel Institute). 2013. *Sheathing braced design of wall studs*. AISI RP13-1. Washington, DC: AISI.

AISI (American Iron and Steel Institute). 2015. *North American standard for cold-formed steel structural framing*. AISI S240. Washington, DC: AISI.

AISI (American Iron and Steel Institute). 2016. *North American cold-formed steel specification for the design of cold-formed steel structural members*. AISI S100-16C. Washington, DC: AISI.

AS/NZS (Australian/New Zealand Standard). 2002. *Structural design actions. Part 0: General principles*. AS/NZS 1170.0. Sydney, Australia: Standards Association of Australia.

ASCE. 2010. *Minimum design loads for buildings and other structures*. ASCE/SEI 7. Reston, VA: ASCE.

ASME. 2003. *Unified inch screw threads, UN and UNR thread form*. ASME B1.1. New York: ASME.

ASTM. 2012. *Standard test methods for evaluating properties of wood-base fiber and particle panel*. ASTM D1037. West Conshohocken, PA: ASTM.

ASTM. 2013. *Standard test methods for tension testing of metallic materials*. ASTM E8/E8M-13a. West Conshohocken, PA: ASTM.

ASTM. 2015. *Standard test methods of conducting strength tests of panels for building construction*. ASTM E72. West Conshohocken, PA: ASTM.

ASTM. 2018a. *Standard specification for steel drill screws for the application of gypsum panel products or metal plaster bases to steel studs from 0.033 in. (0.84 mm) to 0.112 in. (2.84 mm) in thickness*. ASTM C954-18. West Conshohocken, PA: ASTM.

ASTM. 2018b. *Standard specification for steel self-piercing tapping screws for application of gypsum panel products or metal plaster bases to wood studs or steel studs*. ASTM C1002-18. West Conshohocken, PA: ASTM.

ASTM. 2018c. *Standard test methods for structural panels in planar shear (rolling shear)*. ASTM D2718-18. West Conshohocken, PA: ASTM.

IS (Indian Standard). 1995. *Cement bonded particle boards—Specification by Bureau of Indian Standards*. IS 14276. New Delhi, India: Bureau of Indian Standards.

Li, Z., and B. W. Schafer. 2010. "Buckling analysis of cold-formed steel members with general boundary conditions using CUFSM: Conventional and constrained finite strip methods." In *Proc., Int. Spec. Conf. on Cold-Formed St. Structure*. Rolla, MI: Missouri Univ. of Science and Technology.

Madhavan, M., V. Sanap, R. Verma, and S. Selvaraj. 2015. "Flexural strengthening of structural steel angle sections using CFRP: Experimental investigation." *J. Compos. Constr.* 20 (1): 04015018 https://doi.org/10.1061/(ASCE)CC.1943-5614.0000578.

Miller, T. H., and T. M. Peköz. 1994. "Behavior of gypsum-sheathed cold-formed steel wall studs." *J. Struct. Eng.* 120 (5): 1644–1650. https://doi.org/10.1061/(ASCE)0733-9445(1994)120:5(1644).

NAHB (National Association of Home Builders). 1997. *Research commentary on the prescriptive method for residential cold-formed steel framing*. Upper Marlboro, MD: NAHB.

Papangelis, J. P., and G. J. Hancock. 1995. "Computer analysis of thin-walled structural members." *Comp. Struct.* 56 (1): 157–176. https://doi.org/10.1016/0045-7949(94)00545-E.

Peterman, K. D., and B. W. Schafer. 2014. "Sheathed cold-formed steel studs under axial and lateral load" *J. Struct. Eng.* 140 (10): 04014074. https://doi.org/10.1061/(ASCE)ST.1943-541X.0000966.

Pi, Y. L., B. M. Put, and N. S. Trahair. 1999. "Lateral buckling strengths of cold-formed Z-section beams." *Thin Walled Struct.* 34 (1): 65–93. https://doi.org/10.1016/S0263-8231(99)00004-X.

Schafer, B. W. 2006. "Direct strength method (DSM) design guide." In *Committee on specifications for the design of cold-formed steel structural members*. Washington, DC: AISI.

Schafer, B. W., L. C. Vieira Jr., R. H. Sangree, and Y. Guan. 2011. "Rotational restraint and distortional buckling in cold-formed steel framing systems." *Revista Sul-americana de Engenharia Estrutural* 7 (1): 71–90.

Selvaraj, S., and M. Madhavan. 2016. "Enhancing the structural performance of steel channel sections by CFRP strengthening." *Thin Walled Struct.* 108 (Nov): 109–121. https://doi.org/10.1016/j.tws.2016.08.005.

Selvaraj, S., and M. Madhavan. 2017a. "CFRP strengthened steel beams: Improvement in failure modes and performance analysis." *Structures* 12 (Nov): 120–131. https://doi.org/10.1016/j.istruc.2017.08.008.

Selvaraj, S., and M. Madhavan. 2017b. "Strengthening of unsymmetrical open channel built-up beams using CFRP." *Thin Walled Struct.* 119 (Oct): 615–628. https://doi.org/10.1016/j.tws.2017.07.018.

Selvaraj, S., and M. Madhavan. 2018a. "Geometric imperfection measurements and validations on cold-formed steel channels using 3D noncontact laser scanner" *J. Struct. Eng.* 144 (3): 04018010 https://doi.org/10.1061/(ASCE)ST.1943-541X.0001993.

Selvaraj, S., and M. Madhavan. 2018b. "Improvements in AISI design methods for gypsum-sheathed cold-formed steel wall panels subjected to bending." *J. Struct. Eng.* 145 (2): 04018243 https://doi.org/10.1061/(ASCE)ST.1943-541X.0002223.

Selvaraj, S., and M. Madhavan. 2018c. "Studies on cold-formed steel stud panels with gypsum sheathing subjected to out-of-plane bending." *J. Struct. Eng.* 144 (9): 04018136 https://doi.org/10.1061/(ASCE)ST.1943-541X.0002069.

Selvaraj, S., and M. Madhavan. 2019a. "Behaviour of gypsum sheathed point symmetric cold formed steel members: Assessment of AISI design method." *Structures* 22 (Dec): 76–97. https://doi.org/10.1016/j.istruc.2019.06.005.

Selvaraj, S., and M. Madhavan. 2019b. "Bracing effect of sheathing in point-symmetric cold-formed steel flexural members" *J. Constr. Steel Res.* 157 (Jun): 450–462. https://doi.org/10.1016/j.jcsr.2019.02.037.

Selvaraj, S., and M. Madhavan. 2019c. "Design of steel beams strengthened with low-modulus CFRP laminates." *J. Compos. Constr.* 24 (1): 04019052 https://doi.org/10.1061/(ASCE)CC.1943-5614.0000983.

Selvaraj, S., and M. Madhavan. 2019d. "Flexural behaviour and design of CFS wall panels sheathed with particle cement board." *J. Constr. Steel Res* 162 (Nov): 105723. https://doi.org/10.1016/j.jcsr.2019.105723.
Selvaraj, S., and M. Madhavan. 2019e. "Investigation on sheathing effect and failure modes of gypsum sheathed cold-formed steel wall panels subjected to bending." *Structures* 17 (Feb): 87–101. https://doi.org/10.1016/j.istruc.2018.09.013.
Selvaraj, S., and M. Madhavan. 2019f. "Investigation on sheathing-fastener connection failures in cold-formed steel wall panels." *Structures* 20 (Aug): 176–188. https://doi.org/10.1016/j.istruc.2019.03.007.
Selvaraj, S., and M. Madhavan. 2019g. "Retrofitting of steel beams using low-modulus carbon fiber reinforced polymer laminates." *J. Constr. Steel Res.*https://doi.org/10.1016/j.jcsr.2019.105825.
Selvaraj, S., and M. Madhavan. 2019h. "Retrofitting of structural steel channel sections using cold-formed steel encasing channels." *J. Perform. Constr. Facil.* 32 (4): 04018049 https://doi.org/10.1061/(ASCE)CF.1943-5509.0001187.
Selvaraj, S., and M. Madhavan. 2019i. "Sheathing braced design of cold-formed steel structural members subjected to torsional buckling." *Structures* 20 (Aug): 489–509. https://doi.org/10.1016/j.istruc.2019.04.015.
Selvaraj, S., and M. Madhavan. 2019j. "Sheathing bracing requirements for cold-formed steel wall panels: Experimental investigation." *Structures* 19 (Jun): 258–276. https://doi.org/10.1016/j.istruc.2019.01.005.
Selvaraj, S., and M. Madhavan. 2019k. "Strengthening of laterally restrained steel beams subjected to flexural loading using low-modulus CFRP." *J. Perform. Constr. Facil.* 33 (3): 04019032 https://doi.org/10.1061/(ASCE)CF.1943-5509.0001293.
Selvaraj, S., and M. Madhavan. 2019l. "Structural behaviour and design of plywood sheathed cold-formed steel wall systems subjected to out-of-plane loading." *J. Constr. Steel Res.* 166 (Mar): 105888. https://doi.org/10.1016/j.jcsr.2019.105888.
Selvaraj, S., and M. Madhavan. 2019m. "Structural design of cold-formed steel face-to-face connected built-up beams using direct strength method." *J. Const Steel Res.* 160 (Sep): 613–628. https://doi.org/10.1016/j.jcsr.2019.05.053.
Selvaraj, S., M. Madhavan, and S. U. Dongre. 2016. "Experimental studies on strength and stiffness enhancement in CFRP-strengthened structural steel channel sections under flexure." *J. Compos. Constr.* 20 (6): 04016042 https://doi.org/10.1061/(ASCE)CC.1943-5614.0000700.
SFA, SSMA, and AISI (Steel Framing Alliance, Steel Stud Manufacturers Association, and American Iron and Steel Institute). 2007. *Steel framing guide: A builder's guide to steel frame construction*. Washington, DC: Steel Framing Alliance.
Telue, Y., and M. Mahendran. 2001. "Behaviour of cold-formed steel wall frames lined with plasterboard." *J. Constr. Steel Res.* 57 (4): 435–452. https://doi.org/10.1016/S0143-974X(00)00024-9.
Vieira, L. C. M., Jr. 2011. "Behavior and design of cold-formed steel stud walls under axial compression." Ph.D. dissertation, Dept. of Civil Engineering, Johns Hopkins Univ.
Vieira, L. C. M., Jr., and B. W. Schafer. 2012a. "Behavior and design of sheathed cold-formed steel stud walls under compression." *J. Struct. Eng.* 139 (5): 772–786. https://doi.org/10.1061/(ASCE)ST.1943-541X.0000731.
Vieira, L. C. M., Jr., and B. W. Schafer. 2012b. "Lateral stiffness and strength of sheathing braced cold-formed steel stud walls." *Eng. Struct.* 37 (Apr): 205–213. https://doi.org/10.1016/j.engstruct.2011.12.029.
Wang, F., B. Young, and L. Gardner. 2019a. "Compressive testing and numerical modelling of concrete-filled double skin CHS with austenitic stainless steel outer tubes." *Thin Walled Struct.* 141 (Aug): 345–359. https://doi.org/10.1016/j.tws.2019.04.003.
Wang, F., B. Young, and L. Gardner. 2019b. "Experimental study of square and rectangular CFDST sections with stainless steel outer tubes under axial compression." *J. Struct. Eng.* 145 (11): 04019139 https://doi.org/10.1061/(ASCE)ST.1943-541X.0002408.
Wang, L., and B. Young. 2015. "Behavior of cold-formed steel built-up sections with intermediate stiffeners under bending. II: Parametric study and design." *J. Struct. Eng.* 142 (3): 04015151 https://doi.org/10.1061/(ASCE)ST.1943-541X.0001427.
Winter, G. 1960. "Lateral bracing of beams and columns." *J. Struct. Div.* 125 (2): 809–825.
Winter, G., N. Celebi, and T. Peköz. 1972. "Diaphragm braced channel and Z-section beams." In *Center for cold-formed steel structures library.* New York: Cornell Univ.
Ye, J., R. Feng, W. Chen, and W. Liu. 2016. "Behavior of cold-formed steel wall stud with sheathing subjected to compression." *J. Constr. Steel Res.* 116 (Jan): 79–91. https://doi.org/10.1016/j.jcsr.2015.08.028.
Yu, W. W. 2000. *Cold-formed steel design*. Hoboken, NJ: Wiley.
Yura, J. A. 2001. "Fundamentals of beam bracing." *Eng. J.* 38 (1): 11–26.
Zhang, W., M. Mahdavian, Y. Li, and C. Yu. 2016. "Experiments and simulations of cold-formed steel wall assemblies using corrugated steel sheathing subjected to shear and gravity loads." *J. Struct. Eng.* 143 (3): 04016193 https://doi.org/10.1061/(ASCE)ST.1943-541X.0001681.